Radar Image Processing Application Based on Space Cloud Computing in Basketball Game Guidance Camera

Jun Song
School of Physical Education, Qilu Normal University, Ji'nan, China
15805310520@163.com

Submitted: 15 Oct 2024 **Accepted:** 27 Mar 2025 **Published:** 19 May 2025

Abstract Capturing and presenting exciting moments is crucial for the audience's experience in basketball game broadcast cameras. However, traditional radar image processing techniques are limited by various factors and cannot meet the demands of modern audiences for high quality, multi angle, and real-time performance. In response to these challenges, an innovative radar image processing system based on space cloud computing has been proposed. Compared with traditional radar image processing systems, the system proposed by the research institute had the best performance, with accuracy, recall, and F1 value reaching 97.08%, 96.88%, and 97.11%, respectively, and a transmission time of only 2.2 seconds; and the stability was greater than 90%, which was about 10% to 25% higher than other systems. In summary, the system proposed by the research institute has brought revolutionary improvements to basketball game guidance and filming through its efficient processing capabilities, accurate image recognition, fast data processing and transmission, and excellent stability. This not only greatly enriches the audience's viewing experience, but also opens up new directions for the development of sports event broadcasting technology. With the further maturity of technology and the continuous expansion of applications, it is expected that this system will play a more important role in future sports event broadcasting, promoting the development of the entire industry towards higher quality and efficiency.

Keywords: competition guide, space cloud computing, SAR, radar image, image recognition.

1. Introduction and state-of-the-art

Basketball games are one of the most popular sports events in the world, and their broadcast quality has a direct impact on the viewing experience of the audience [31]. To ensure high-quality broadcasting, the director's camera often relies on monitoring equipment such as radar to assist in locating and tracking the dynamics of athletes and basketballs when completing the shooting and switching of live footage [17]. This technical support enables the director's camera to perform precise shooting, ensuring real-time capture and smooth transmission of images, thereby enhancing the audience's viewing experience [4,27]. Synthetic Aperture Radar (SAR) is an advanced radar system known for its high resolution, capable of precise remote detection of ground and ocean targets, and real-time imaging [33]. These capabilities have enabled SAR to be widely applied in various fields, such as military reconnaissance, geological surveys, environmental monitoring, etc. Sleem et al. combined the historical time series of SAR with the latest geotechnical data to monitor the causes of ground instability in the Ismailia region. They processed 25 ENVISAT ASAR scenarios and 77 differential interferograms.

The ground instability in Ismailia District was mainly controlled by three basic parameters: groundwater depth, clay layer depth, and expansion potential [30]. To analyze the vegetation status in agricultural monitoring, Kumar derived a new vegetation index from dual polarized SAR data using scattering information from polarization degree and eigenvalue spectrum. The vegetation index of rapeseed had the highest correlation with biophysical variables, with determination coefficients of 0.79, 0.82, and 0.75 for plant area index, vegetation moisture content, and dry biomass, respectively [18]. Hati et al. used SAR data to estimate the aboveground biomass of highly complex mangrove communities on the Indian island of Lothian. The aboveground biomass of Lothian Island ranged from 1.15 tons/hectare to 79.83 tons/hectare, with an average of 20.23 tons/hectare [13]. Kikon et al. used differential SAR interferometry to estimate the frequency of surface deformation in Kohima District, Nagaland State, India in 2018 and 2019, in response to the shortcomings of existing surface deformation detection technologies. The subsidence rate in Koshima County was relatively high in 2018, with higher subsidence rates in the southern and western regions compared to the northern and eastern regions [16].

Although SAR technology is essential in multiple fields with its rapid data processing capabilities, wide monitoring range, and excellent resolution, the large amount of data and high-density data streams it collects pose a huge challenge for real-time data processing [8]. The introduction of cloud computing technology provides a new solution to this problem. Oh et al. proposed a privacy protection data collection method based on mobile cloud computing technology to ensure the secure storage of user information and prevent data from being easily tampered with. The proposed method improved the delay efficiency by 170% [26]. Li conducted research on the Chinese translation of literary works using artificial intelligence and machine learning capabilities on cloud computing platforms to decipher cultural translation. This method revealed the subtle relationship between the Chinese translation of literary works and the content before and after translation by focusing on the semantic relationships between words [20]. Madankan used queue theory to model cloud computing to measure the service quality of computer services. The arrival rate and service rate of the processing server were the two main parameters that affected the performance of the model. By modeling the queue network of the cloud platform, it was easy to determine and measure the service quality of computer services [23]. Ding et al. designed a space-based embedded cloud computing platform to address the limitations of existing cloud computing technologies in fully utilizing storage and computing resources, and to meet the application requirements of space-based intelligent computing and ground-based cloud computing systems. This platform not only performed well in processing large-scale data, but also had significant advantages in ensuring real-time and reliability of computing tasks [9]. Alsharari et al. proposed a cloud computing method based on cloud enterprise resource planning to explore the impact of contingency factors on the public sector in the United Arab Emirates. The calculation results showed that institutional pressure in highly institutionalized environments could

Tab. 1. Summary of relevant studies.

Radar image processing technology	Publication	Research content	Research result
Supervised multi-view hash model	Yan et al. [36]	Enhancing multi-view information by neural networks.	The research methodology significantly outperforms state-of-the-art single-view and multi-view hashing methods.
Group-based nuclear norm and learning graph (GNNLG) model	Yan et al. [38]	In order to collect similarities between patches more efficiently	The proposed method is superior to the current state-of-the-art image denoising methods in terms of both subjective and objective criteria.
Task Adaptive Attention Module for Image Captioning	Yan et al. [37]	To mitigate the misdirection of traditional attention mechanisms	Inserting a task-adaptive attention module into a dummy-transformer-based image caption model improves model performance.
Precision reference-free image quality assessment programme	Yan et al. [41]	To address the shortcomings of the lack of understanding of image distortion in non-referenced image quality assessment (NR IQA)	Aberration classification accuracy of the research method is higher than that of state-of-the-art aberration classification methods.
Multi-feature Fusion and Decomposition (MFD) Framework	Yan et al. [39]	In order to be able to learn more discriminative and robust features of images and to reduce intra-class variation.	Image recognition performance is significantly improved.
Space-based embedded cloud computing platform	Ding et al. [9]	Addressing the shortcomings of existing cloud computing technologies where storage and computing resources cannot be fully utilised	The platform not only excels in processing large-scale image data, but also has significant advantages in ensuring the real-time and reliability of computational tasks.

generate organizational responses, but these responses depended on various aspects of organizational culture and are influenced by it [2]. In order to visually compare the differences between various image processing techniques, the study summarizes them. An overview of the research related to image processing techniques is shown in Table 1.

In summary, the current radar image processing technology generally still faces the

problems of insufficient data processing capacity and limited storage capacity, which can not ensure the real-time capture and smooth transmission of the picture in the basketball game guide camera. In addition, it also has the problems of insufficient resolution and high delay in basketball game broadcasting. Insufficient resolution will lead to blurred images, which cannot clearly show the movement of the athletes and the trajectory of the ball; high latency will affect the real-time performance, and the audience may see images that are inconsistent with the actual event. At the same time, radar signals are susceptible to environmental interference, leading to inaccurate target tracking, and the computational burden of data fusion and processing also increases the complexity of the system. Based on this situation, this study innovatively proposes a system architecture based on space cloud computing technology, and utilizes the flow of state diagrams to implement complex SAR imaging processing flow. Finally, this study proposes a radar image processing system based on space cloud computing architecture and variable scale imaging algorithm. The purpose of this study is to meet the precise shooting needs of basketball games by the director's camera and improve the real-time performance of SAR imaging processing.

This study is divided into three parts. The next part (Section 2) introduces how space cloud computing, SAR imaging algorithms, and the overall system framework are improved, as well as how the radar image processing system is established. The following part (Section 3) describes the performance testing of the new system, and the last part (Section 4) is a conclusion of the article.

2. Methods and materials

In response to the problems existing in the current basketball game broadcast camera, the study first introduces the principle of SAR system radar imaging, and proposes a multi star index based variable scale imaging algorithm by introducing SAR imaging algorithm. In addition, the combination of space cloud computing and multi satellite collaborative work has been utilized, and a SAR overall framework based on space cloud computing has been constructed. Finally, a new radar image processing system based on space cloud computing architecture is established, which is based on the overall framework of SAR using space cloud computing and the variable scale imaging algorithm using multi star indexing.

2.1. Selection and improvement of SAR imaging algorithms

In the field of radar imaging, researchers and technology developers have always pursued high resolution as one of their core goals. High resolution capability can make the observation and recognition of target details clearer, which is particularly important in basketball game guidance cameras [11, 12]. Because clear images not only enhance the visual experience of the audience, but also provide more accurate information on the

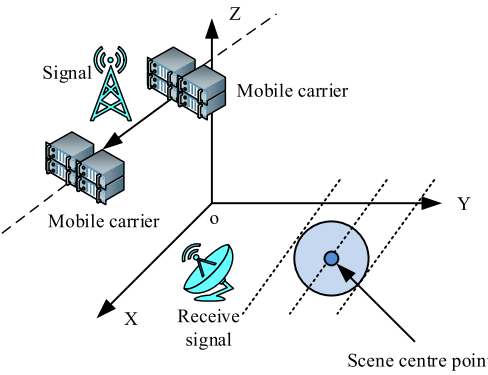

Fig. 1. Radar imaging principles for SAR system.

athlete's position and movement trajectory [44]. SAR systems can significantly improve imaging resolution without increasing the physical antenna size by simulating larger antenna apertures [14]. The radar imaging principle of SAR system is shown in Figure 1. In this Figure, SAR imaging is based on a basic principle: a moving carrier moves along a straight line in a specific direction at a constant speed, continuously emitting pulse signals at a fixed frequency to the target area. At the same time, the receiving device carried by the carrier continuously captures and fully records the echo signals reflected by the target [6]. The SAR imaging algorithm is the core of efficient data processing in SAR systems [3]. In this process, SAR imaging algorithms not only ensure the accuracy and efficiency of data processing, but also play a crucial role in improving the resolution and reliability of images [24]. The widely used SAR imaging algorithm currently is the range Doppler algorithm, however, this algorithm only focuses on the impact of distance curvature on imaging and ignores the influence of distance curvature differences in the scene [21,35]. In response to this situation, this study improved the SAR imaging algorithm and proposed a multi-scale imaging algorithm based on multi star indexing. The data transmission process of this algorithm in the spaceborne radar SAR imaging processing is shown in Figure 2. In this Figure, the algorithm proposed in this study adopts the strategy of distributing data processing tasks from the main satellite to the auxiliary satellite in the imaging processing of spaceborne radar SAR. In the data transmission stage, the main satellite evenly divides the data to be processed into four parts, and then sends the corresponding data segments to the corresponding auxiliary satellites according to their respective serial numbers. The auxiliary satellites involved in this process include satellites numbered 1, 2, 3, and 4, all of which undertake the comprehensive processing of the algorithm in both distance and azimuth directions. In addition, the main satellite is responsible for transmitting the independent variable values

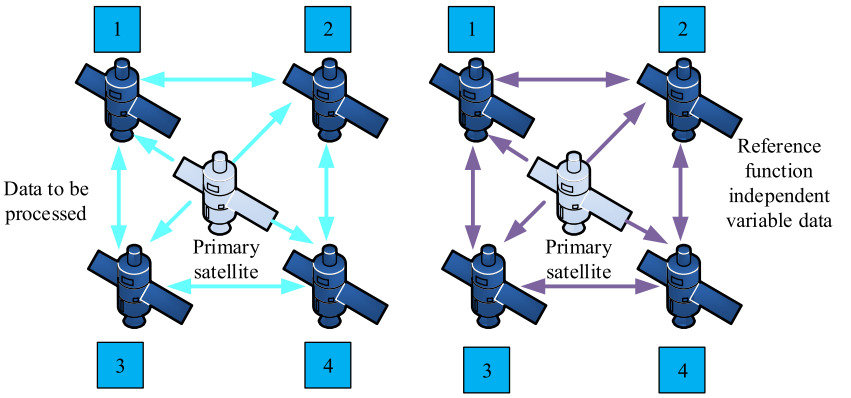

Fig. 2. Data transfer flow during SAR imaging processing.

of all reference functions to these auxiliary satellites separately to ensure consistency and accuracy in data processing.

2.2. Overall framework structure design of SAR based on space cloud computing

Space cloud computing is an emerging technology concept that deploys computing resources in space to achieve real-time processing and analysis of Earth observation data, providing near real-time data processing capabilities. This is particularly important for application scenarios that require rapid response, such as real-time guidance and filming of basketball games [5,7]. The service types of space cloud computing mainly include edge computing as a Service (ECaaS), Infrastructure as a Service (IaaS), Network as a Service (NaaS), Platform as a Service (PaaS) and Software as a Service (SaaS) [1]. These service types can be selected and combined according to the specific needs and application scenarios of users to achieve the best cloud computing solution [43]. However, spaceborne radar SAR imaging technology has extremely high standards for data processing capabilities, which often exceed the capabilities of a single spaceborne processing platform. So it is necessary to achieve excellent data processing capabilities through the collaborative work of multiple satellites [15,42]. Therefore, this study built a multi satellite space cloud computing processing platform based on satellite collaborative work. The structure of the multi satellite space cloud computing processing platform is shown in Figure 3. In this Figure, the multi satellite space cloud computing processing platform proposed by the research institute consists of multiple small satellites, such as the main satellite, small satellite 1, small satellite 2, small satellite 3, and small satellite 4 in Figure 3. These satellites work together to form a network that covers a wider detection area. Satellites transmit data through laser communication technology, which ensures high bandwidth

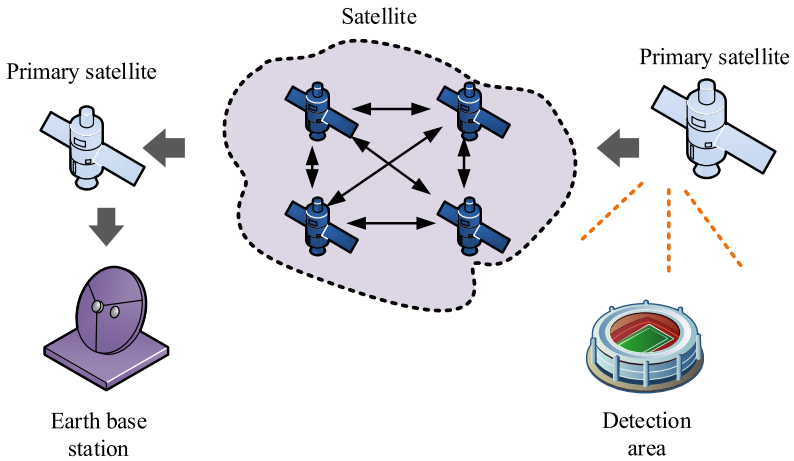

Fig. 3. Architecture of a multi-satellite space cloud computing processing platform.

and low latency. Therefore, satellites can transmit detected data in real-time, ensuring the timeliness of data processing and jointly completing the real-time imaging processing task of the entire spaceborne SAR. Linear Frequency Modulated (LFM) algorithm is a widely used signal processing technique in radar systems. By analyzing the frequency changes of the echo signal, the distance and relative velocity of the target can be determined. It is very suitable for high-resolution imaging processing of spaceborne SAR for long-distance migration [10, 34]. Therefore, based on the multi satellite space cloud computing processing platform, this study introduces the LFM algorithm and utilizes the flow of state diagrams to implement a complex SAR imaging processing flow. The mapping relationship between processes is shown in Figure 4. In this Figure, the processing flow of LFM is implemented through 11 state diagrams. The main satellite and the small satellite cycle three times in three stages, namely the main satellite waiting for reply stage, the small satellite processing subtask stage, and the waiting for the next stage instruction stage. In the first stage, the main satellite is responsible for distributing raw data and task instructions, while the small satellites perform operations such as FFT, linear frequency modulation, and matrix transposition. In the second stage, the main satellite updates tasks according to instructions. In the third stage, the small satellite completes the IFFT and returns the results, while the main satellite collects and confirms the completion of the task, and carries out subsequent operations according to the instructions of the ground control center. Therefore, to meet the task and functional design of master-slave satellites, this study combines a multi satellite space cloud computing processing platform, LFM algorithm, and state diagram flow to construct a SAR overall framework structure based on space cloud computing. The expression for

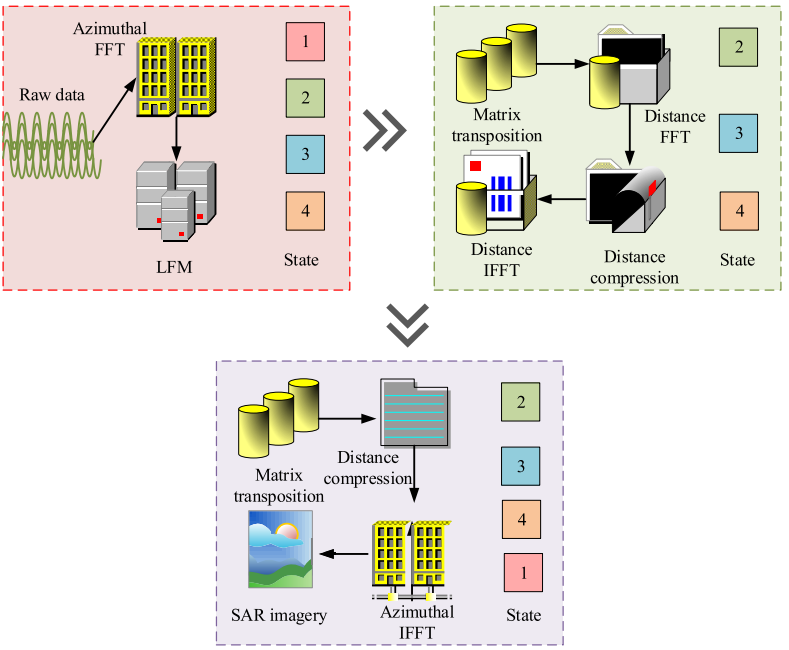

Fig. 4. Mapping between the flow of multi-satellite connectivity state charts and the processing flow of the LFM algorithm.

calculating the linear frequency modulation signal $s(\hat{t}, t_m)$ is shown in equation (1):

$$s(\hat{t}, t_m) = \text{rect}\left(\frac{\hat{t}}{T_p}\right) = \exp\left[j2\pi\left(f_c t + \frac{1}{2}\gamma\hat{t}^2\right)\right], \tag{1}$$

where t, $\hat{t}$ and t_m represent full time, distance fast time, and azimuth slow time, respectively; $\text{rect}(\cdot)$ represents rectangular window function; f_c and γ represent modulation frequency and signal carrier frequency, respectively; T_p represents pulse width. Phase is a fundamental part of a signal and instantaneous phase is used to describe how the frequency of a signal changes over time. The instantaneous phase of the LFM algorithm up converted waveform $\psi(t)$ calculation expression is shown in equation (2):

$$\psi(t) = 2\pi(f_o t + \frac{1}{2}\gamma t^2), \tag{2}$$

where f_o represents the center frequency of the carrier signal, indicates the fundamental frequency of the signal without FM. The expression for calculating the instantaneous

frequency $f(t)$ is shown in equation (3):

$$f(t) = \frac{1}{2\pi}\frac{d}{dt}\psi(t) = f_o + \gamma t\,. \tag{3}$$

The expression for distance resolution N is shown in equation (4):

$$N = \frac{R_m - R_n}{\Delta R}\,, \tag{4}$$

where R_m, R_n, and ΔR represent the maximum distance, minimum distance, and the distance difference between two targets, respectively. The expression for the azimuth target distance $R_a(t_m)$ is shown in equation (5):

$$R_n(t_m) = \sqrt{R_s^2 + (Vt_m - X_n)^2}\,, \tag{5}$$

where V represents the speed of the carrier platform motion; t_m represents slow time sampling; R_s and X_n, respectively, represent the vertical distance of the carrier motion direction and the X coordinate of point n. The expression for the fundamental frequency echo $s_n(t_m)$ is shown in equation (6):

$$s_n(t_m) = \sigma_n e^{-j\frac{4\pi R_n(t_m)}{c} f_c}\,, \tag{6}$$

where σ_n represents the amplitude of the signal. The phase transformation of the echo in the azimuth direction $\varphi_n(t_m)$ is calculated as shown in equation (7):

$$\varphi_n(t_m) = \frac{-4\pi f_c}{c}[R_n(t_m) - R_s]\,, \tag{7}$$

where c represents the speed of light propagation. The expression for calculating the Doppler frequency f_d is shown in equation (8):

$$f_d = \frac{2f_c V}{c}\sin\theta_n\,, \tag{8}$$

where θ_n represents the oblique angle of view. The Doppler bandwidth Δf_d is calculated as shown in equation (9):

$$\Delta f_d = \frac{2V}{D}\,, \tag{9}$$

where D represents the transverse aperture length. The expression for calculating the phase function $H_1(\hat{t}, f_a, R_s)$ by changing the linear frequency modulation scale is shown in equation (10):

$$H_1(\hat{t}, f_a, R_s) = \exp\left[j\pi\gamma_e(f_a, R_B)a(f_a)\left(\hat{t} - \frac{2R(f_a, R_B)}{c}\right)^2\right]\,, \tag{10}$$

where f_a and R_B, respectively, represent the Doppler frequency and the shortest distance from point n to the flight path, and $a(\cdot)$ represents the echo response envelope.

2.3. Construction of radar image processing system based on space cloud computing architecture

When satellites conduct uninterrupted and all-weather monitoring, the obtained satellite image data is very large, and traditional radar image processing systems cannot meet the processing needs of heavy load data [19, 25, 40]. Therefore, based on the powerful computing and analysis capabilities of the SAR overall framework using space cloud computing, as well as the high-resolution advantages of the multi star index based variable scale imaging algorithm, a new radar image processing system based on space cloud computing architecture has been established in this study. The system mainly consists of fiber optic transmission module, DDR3 SDRAM storage module, FFT operation module, multiplication module, and data stream. This design is able to overcome the limitation that the traditional system is unable to handle the huge satellite image data. Through the cooperation of fiber optic transmission, DDR3 SDRAM storage, FFT operation and multiplication module, it can not only effectively improve the speed and accuracy of data processing, optimize the management of data flow, but also solve the problem of high load data processing and transmission. These improvements enable the new system to have higher processing efficiency, image quality and real-time performance, which can show obvious advantages when facing large data volume and complex tasks.

The structure of the DDR3 SDRAM storage module is shown in Figure 5, in which this storage module in the new research system mainly consists of four front-end First In First Out (FIFO) data structures, four back-end FIFOs, one interface FIFO, and four partition memories. The write operation of data in partition memory 1 is only performed by the front-end FIFO1 and transmitted through the interface FIFO, ultimately stored in the corresponding partition memory 1 address of DDR3 SDRAM. Similarly, data in partitioned memory 1 can only be read through backend FIFO1. The data writing and reading process for partition memory 2, partition memory 3, and partition memory 4 follows the same operational flow as that for partition 1.

The working state flow of the DDR3 SDRAM storage module during data read and write operations is shown in Figure 6. The DDR3 SDRAM storage module first enters an idle state before performing data read and write operations, and while refreshing parameters, checks whether the front-end FIFO is waiting to process data. If there is data in the frontend FIFO, the module will check if there is enough space in the current area to store this data. If there is enough space, the module will read data from the front-end FIFO and perform DDR3 write operations. After writing is completed, the module will update the parameters. If there is no data in the front-end FIFO or the current area space is insufficient, the module will check whether there is data in the back-end FIFO. If there is, the module will detect whether there is data inside DDR3 and perform a read operation. After the read operation is completed, the module updates its parameters and prepares to switch to the next area.

The algorithm processing flow in the radar image processing system based on space

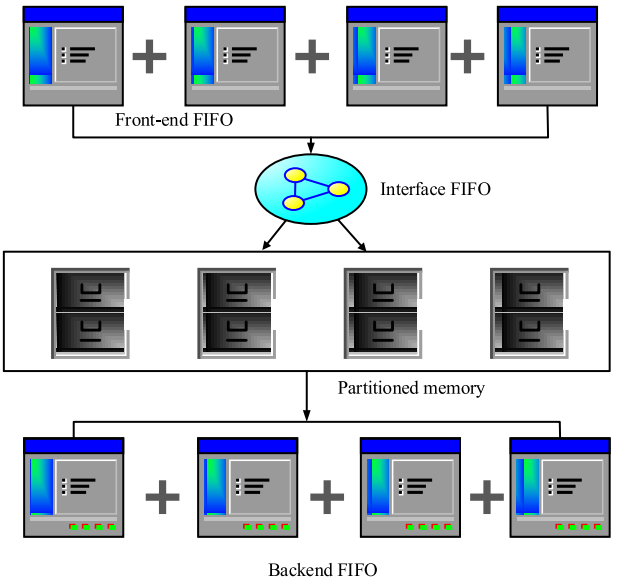

Fig. 5. Architecture of DDR3 SDRAM memory modules.

cloud computing architecture is shown in Figure 7. The new radar image processing system constructed by the research institute performs algorithm processing in five stages. Firstly, the upper computer software sends SAR data and related variables to the first processing unit via optical fiber. Next, the system performs azimuth FFT and performs complex multiplication using the reference function H1. Then, the data is transposed, subjected to distance compression and correction, and multiplied by H2. Afterwards, the data is converted to the time domain through IFFT and stored in DDR3 SDRAM. Finally, the imaging data is transmitted back to the upper computer through optical fibers for image display and subsequent processing. The definition of FFT is shown in equation (11):

$$X(k) = \sum_{n=0}^{N-1} x(n) \exp(-jnk2\pi/N)\,, \tag{11}$$

where N is the conversion length. The inverse definition of FFT $x(n)$ is calculated as shown in equation (12).

$$x(n) = \frac{1}{N} \sum_{k=0}^{N-1} X(k) \exp\left(j2\pi \frac{nk}{N}\right)\,. \tag{12}$$

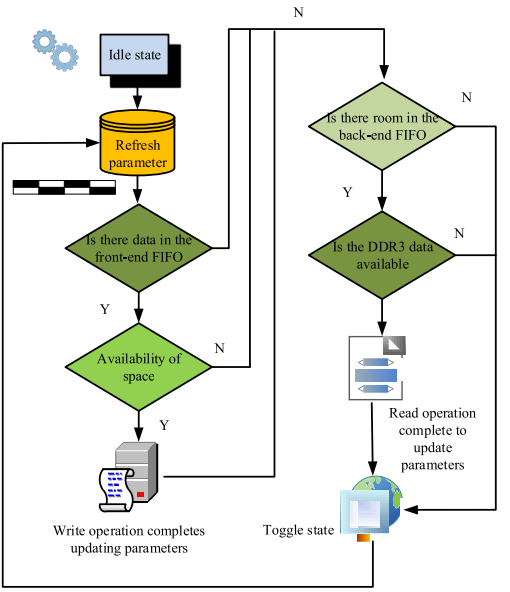

Fig. 6. DDR3 SDRAM memory module operating state flow.

Radar image processing systems based on space cloud computing architectures usually also face high time complexity and space complexity. In terms of time complexity, SAR image processing requires a large number of computations, such as Fourier transform, etc., and the computation time grows significantly as the data volume increases. In order to improve efficiency, the system utilises distributed computing resources to process large data volumes in parallel and reduce the computational burden of a single node. In terms of space complexity, the storage requirement of SAR images is proportional to the resolution, and the huge storage volume of high-resolution images requires efficient storage systems (e.g., DDR3 SDRAM) and data compression techniques to manage the data. It is recommended to use at least 8-core processors with at least 3.0 GHz clocks, such as AMD Ryzen 9 7950X or Intel Core i9-13900K, paired with at least 64 GB of RAM (DDR4/DDR5). For GPU, NVIDIA A100 Tensor Core or NVIDIA V100 is recommended with 40 GB/80 GB HBM2 memory and 6912 CUDA cores to support parallel computing and deep learning acceleration to improve image processing efficiency. For storage, use high-performance SSDs such as Samsung 970 PRO 2 TB or Intel Optane SSD 905P 1.5 TB with DDR4 3200 MHz or DDR5 4800 MHz memory (64 GB or 128 GB) to ensure fast data access and high-bandwidth through Fibre Channel or InfiniBand data transfer.

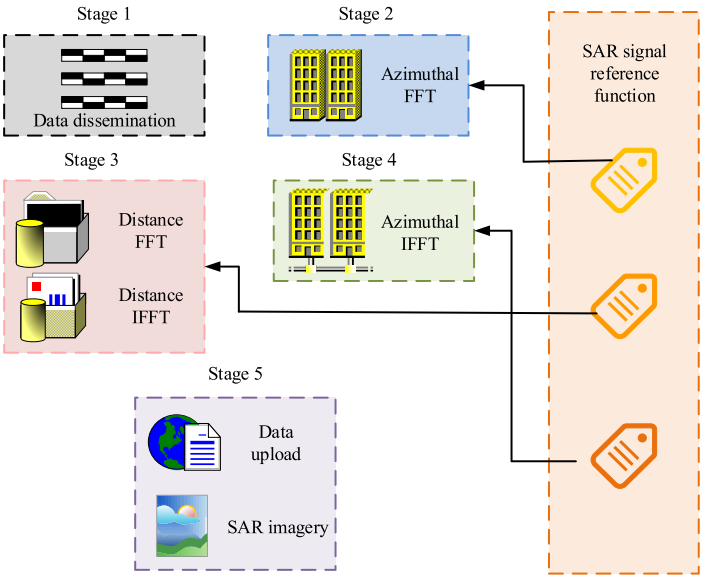

Fig. 7. Algorithmic process handling in radar image processing system based on space cloud computing architecture.

3. Results

To verify the performance of the new SAR imaging algorithm and the radar image processing system based on space cloud computing architecture, this study first sets up a suitable experimental environment and preprocessed the test data. Secondly, the proposed method was tested through comparative testing of the same type and multi criteria performance testing. After completion, the new research system was simulated and tested using actual basketball game guidance camera data.

3.1. SAR imaging algorithm performance testing

This study was based on the Windows operating system, and the XC7VX485T chip from the Virtex-7 FPGA series of Xilinx was selected as the core processor. The CPU was Intel Core i9-13900K and the GPU was NVIDIA V100. The test data came from the GMTSAR dataset [28, 29] and a synthetic DORiSAR dataset generated via SAR imaging simulator, using parameters similar to Sentinel-1 acquisition geometry [22]. These datasets were divided into training and testing sets in a 6 : 4 ratio. Matlab [32] was used to set 5 point targets, where pulses were emitted and echo signals were generated.

Tab. 2. Important parameter settings during the imaging process.

Serial number	Parameter name	Numerical value
1	Radar carrier frequencies	5.4×10^9
2	Azimuthal sampling rate	1257.02
3	Radar sampling rate	3.26×10^7
4	Pulse time width	4.22×10^{-5}
5	Distance-directed frequency	7.19×10^{11}
6	Nearest radar to target	9.91×10^5
7	Radar equivalent velocity	7064
8	Doppler centre frequency	−6893
9	Data window start time	6.61×10^{-3}

Then, the echo signals were filtered and denoised, and the images were generated by frequency domain transformation using FFT. A variable scale imaging algorithm based on multiple star indexes was applied to improve the image resolution and clarity. The data was accessed through a DDR3 SDRAM memory module and a fibre optic transmission module ensureed fast data flow. Finally, the training set optimised the algorithm and the test set verified the performance to ensure the stability and real-time response of the system under different conditions.

The important parameter settings during the imaging process are shown in Table 2. Based on these values, this study introduced popular SAR imaging algorithms of the same type for comparison, namely the Focused Synthetic Aperture Radar (FSAR), the Synthetic Aperture Radar Interferometer SAR (InSAR), and the Polarimetric Synthetic Aperture Radar (PolSAR).

Firstly, the image quality evaluation index, Structural Similarity Index (SSIM), was used to compare different imaging algorithms. The test results are shown in Figure 8. In this Figure it can be seen that, whether in the GMTSAR dataset or the DORiSAR dataset, the SAR imaging algorithm performed the best, followed by the PolSAR algorithm and InSAR algorithm, and the FSAR algorithm performed the worst. In Figure 8a, the maximum SSIM values for FSAR algorithm, InSAR algorithm, PolSAR algorithm, and the proposed algorithm in the GMTSAR dataset were 0.69, 0.75, 0.89, and 0.96, respectively. In Figure 8b, the maximum SSIM values for the four algorithms in the DORiSAR dataset were 0.61, 0.88, 0.91, and 0.99, respectively. The above data indicates that the research algorithm had significant advantages in maintaining image structure and quality. It improved the SAR imaging algorithm by using a multi star index variable scale imaging method, which could effectively enhance the algorithm's efficiency in maintaining image quality. In addition, SAR images with high SSIM values

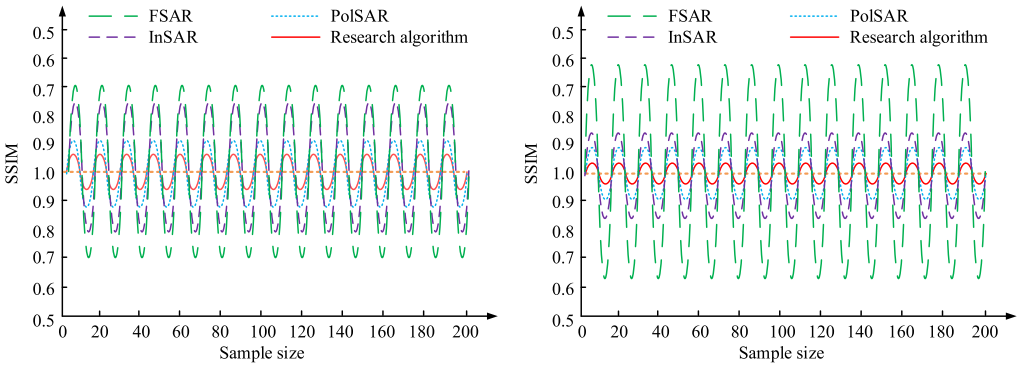

a GMTSAR **b** DORiSAR

Fig. 8. Comparison of SSIM performance tests of different SAR imaging algorithms.

provided reliable data support for subsequent experiments, ensuring the accuracy and reliability of the experimental results.

To confirm the resolution capability of the proposed algorithm, the four SAR imaging algorithms were tested using image clarity as the indicator. The test results are shown in Figure 9. In the images shown in this Figure it can be seen that the result from the research algorithm (Fig. 9b) was visually very close to that of the original image (Fig. 9a), and it was almost impossible to observe significant quality differences with the naked eye. The clarity of radar images obtained by PolSAR algorithm, InSAR algorithm, and FSAR algorithm (Figs. 9c-9e) differed significantly from the original images, especially the radar image obtained by FSAR algorithm (Fig. 9e). From this it follows that the research algorithm performed better in radar image resolution than PolSAR, InSAR, and FSAR algorithms, demonstrating its potential and advantages in the field of radar image processing.

In addition, to explore the real-time capture capability of the proposed algorithm, the data processing speed of the four algorithms mentioned above was also tested. The test results are shown in Figure 10. It can be seen in this Figure that the research algorithm exhibited fast data processing speed in both datasets. Within the range of increasing the sample size from 20 to 200, the data processing speed of all algorithms decreased, but the research algorithm still maintained a relatively fast speed. In Figure 10a, the shortest data processing speeds for FSAR algorithm, InSAR algorithm, PolSAR algorithm, and the research algorithm were 14.9 s, 14.2 s, 12.7 s, and 5.6 s, respectively. In Figure 10b, the shortest data processing speeds for FSAR algorithm, InSAR algorithm, PolSAR algorithm, and the research algorithm were 14.5 s, 14.0 s, 10.9 s, and 5.0 s, respectively. The above data indicate that the research algorithm had good efficiency, scalability, and excellent real-time performance in processing large-scale SAR data.

a Original

b Research algorithm

c PolSAR

d InSAR

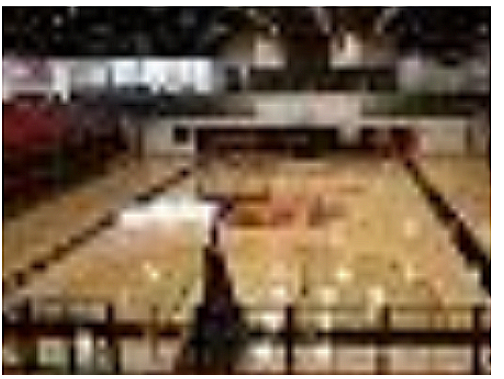

e FSAR

Fig. 9. Radar image clarity experiment comparison results.

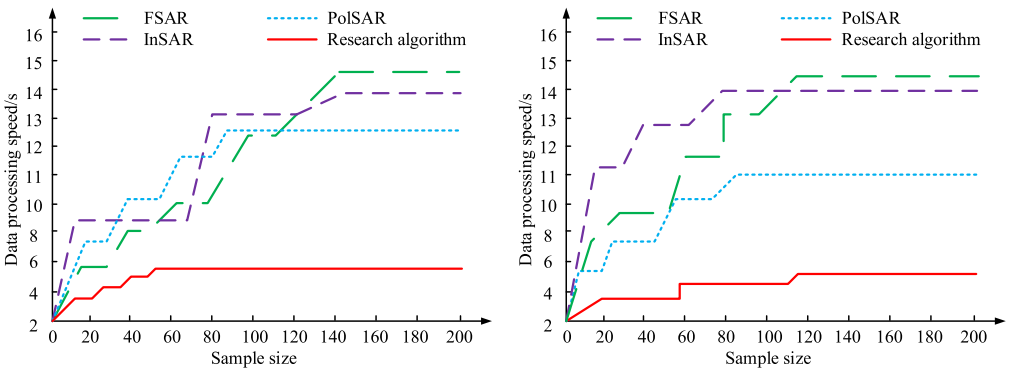

a GMTSAR **b** DORiSAR

Fig. 10. Comparison results of data processing speed test for different SAR algorithms.

3.2. Simulation testing of radar image processing system based on space cloud computing architecture

This study used actual observation data obtained from spaceborne SAR for simulation analysis. The SAR image data had 8192 pixels in both distance and azimuth directions, and each pixel was composed of a real and imaginary part represented by a 32-bit single precision floating-point number, forming complex data. Therefore, the total capacity of the entire dataset reached 512MB, and the dataset was divided into training and testing sets in a 6 : 4 ratio. To better reflect the imaging performance of the research system, this study also introduced traditional Extended Azimuth Non Linear Variable Scaling Radar Processing System (EANLVSRS), Doppler Radar Processing System (DRPS), and Frequency Modulated Continuous Wave Radar (FMCW) image processing systems. The ground target is selected with a 3×3 uniform point array. The simulation scene is shown in Figure 11.

Based on the simulation scenario shown in Figure 11 and the actual observation data obtained, the data was normalized and cleaned. Random sampling was conducted for multi index testing with precision, recall, F1 value, and transmission time as reference indicators. The test results are shown in Table 3. According to these results, the research system demonstrated high accuracy, high recall, and high F1 score on both the training and testing sets, while also having the shortest transmission time. On the training set, its accuracy, recall, and F1 score were 96.84%, 95.59%, and 96.64%, respectively, with a transmission time of 2.6 seconds; On the test set, its accuracy, recall, and F1 score were 97.08%, 96.88%, and 97.11%, respectively, with a transmission time of 2.2 seconds. The EANLVSRS system performed the worst on both the training and testing sets. On the training set, its accuracy, recall, and F1 score were only 68.36%, 67.08%, and 68.55%,

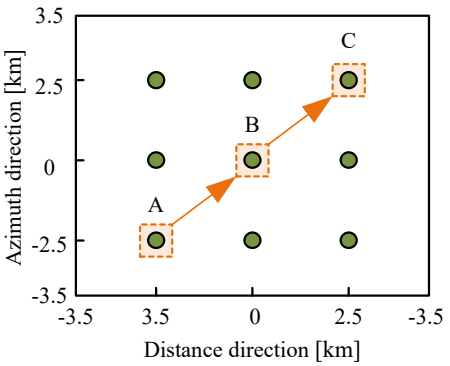

Fig. 11. Simulation scenario.

Tab. 3. Comparison of test results with various indicators. A: accuracy, R: recall, F1: F1 score.

Data set	System	A [%]	R [%]	F1 [%]	Transmission time [s]
Training set	EANLVSRS	68.36	67.08	68.55	15.2
	DRPS	72.57	71.55	72.85	12.1
	FMCW	82.45	80.22	83.53	11.6
	Research system	96.84	95.59	96.64	2.6
Test set	EANLVSRS	69.65	68.37	70.11	14.6
	DRPS	73.54	72.08	73.02	11.9
	FMCW	83.55	82.53	82.88	11.3
	Research system	97.08	96.88	97.11	2.2

respectively, with a transmission time of 15.2 seconds; On the test set, its accuracy, recall, and F1 score were 69.65%, 68.37%, and 70.11%, respectively, with a transmission time of 14.6 seconds. Compared with the research system, the accuracy, recall, and F1 value of the EANLVSRS system had been reduced by about 28%, and the transmission time had been extended by about 13 seconds. From this, the real-time data processing capability of space cloud computing and the ability to simplify complex processes through multi satellite connection state diagrams effectively improved the responsiveness of radar image processing systems, promoting the research system to have good multi index performance effects.

To confirm the stability of the system during operation, we have continued to test the performance of the four systems mentioned above. The test results are shown in Figure 12. As it can be seen in the graphs shown in this Figure, the stability of all four

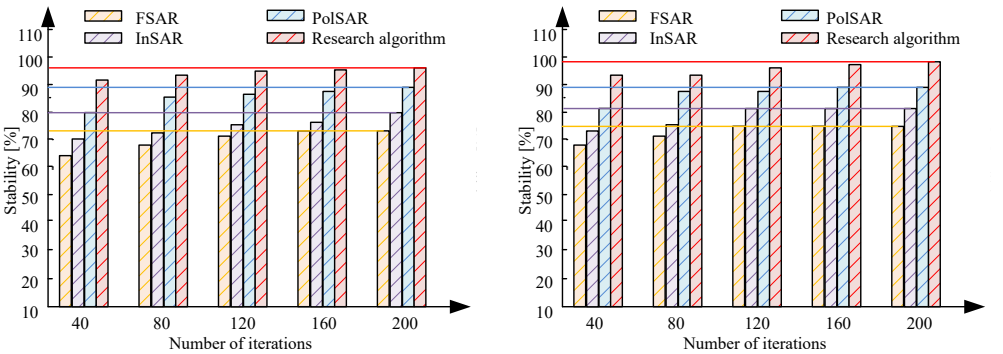

a GMTSAR **b** DORiSAR

Fig. 12. Comparison of results for stability of different radar image systems.

Tab. 4. Comparison of running time of different systems.

Data set	Systems	1st [s]	2nd [s]	3rd [s]	4th [s]	5th [s]	6th [s]	7th [s]
Training set	EANLVSRS	15.2	15.6	15.8	16.1	16.2	16.8	17.0
	DRPS	12.1	12.2	12.5	12.7	12.8	13.0	13.5
	FMCW	11.6	11.8	12.1	12.2	12.5	12.6	12.8
	Research system	2.6	2.8	3.0	3.2	3.4	3.6	3.7
Test set	EANLVSRS	14.6	14.8	14.9	15.3	15.8	15.6	16.0
	DRPS	11.9	12.1	12.3	12.8	13.0	13.2	13.4
	FMCW	11.3	11.5	11.6	11.7	11.9	12.1	12.3
	Research system	2.2	2.3	2.4	2.6	2.7	2.9	3.0

systems slowly increased with the increase of iteration times. The research system had the best stability effect, with stability greater than 90% in both the training and testing sets. The highest stability of the EANLVSRS system, DRPS system, and FMCW system was only 74.9%, 81.3%, and 89.6%, respectively. Compared with the research system, the stability of the other three systems decreased by about 10% to 25%. From the above data it follows that the research system not only had high accuracy in processing radar images, but also had significantly better stability than other systems, indicating that it had higher reliability and robustness in practical applications.

In this study we have also compared the operational complexity of the different systems mentioned above. The test results are shown in Table 4. The running times of different systems gradually increased with the number of executions. The running time of EANLVSRS, DRPS, FMCW, and research system in the training set increased by

Tab. 5. Metrics test results for different models. Resource consumption rate (Resource CR) refers to the relative proportion of computing resources (such as CPU, memory, electrical energy, etc.) consumed by the system during the execution of image processing tasks, reflecting the efficiency and overhead of the system operation.

Environments	Systems	MSE	MAE	Resource CR [%]	Accuracy [%]
Rainy	EANLVSRS	0.078	0.081	23.33	80.83
	DRPS	0.072	0.066	20.16	84.04
	FMCW	0.065	0.057	18.65	91.24
	Research system	0.033	0.028	7.43	96.89
Cloudy	EANLVSRS	0.063	0.064	20.44	84.12
	DRPS	0.057	0.052	19.32	87.84
	FMCW	0.041	0.045	17.25	91.58
	Research system	0.028	0.029	6.84	97.71
Sunny	EANLVSRS	0.054	0.052	20.13	86.49
	DRPS	0.048	0.049	18.87	89.36
	FMCW	0.038	0.040	15.36	92.75
	Research system	0.021	0.022	6.65	98.23

1.8 s, 1.4 s, 1.2 s, and 1.1 s, respectively; The running time in the test set increased by 1.4 s, 1.5 s, 1.0 s, and 0.8 s, respectively. However, the increase was very small and did not affect the overall performance of the system. The research system had the shortest running time, only 3.0 seconds; FMCW system was second, with a duration of 12.3 s; The EANLVSRS system had the longest running time, which was 16.0 s. From this it follows that the research system was computationally simple and could efficiently process basketball game guidance camera data. The main reason for this was the powerful computing and analysis capabilities of the SAR overall framework based on space cloud computing, which had greatly improved the transmission and operation efficiency.

Finally, in order to investigate the effect of environment on the system, in this study we have also compared the above four systems for rainy, cloudy and sunny environments using Mean Squared Error (MSE), Mean Absolute Error (MAE), resource consumption rate and image processing accuracy as reference indicators. The test results are shown in Table 5. As can be seen in this Table, whether in rainy, cloudy or sunny environments, the EANLVSRS system has the worst performance of the four systems in terms of various metrics. The performance of DRPS, FMCW and the radar image processing system with the new space cloud computing architecture proposed by the Institute varies from low to high, and intuitively, it can be found that the research system has the lowest MSE value of 0.021, the lowest MAE value of 0.022, the lowest resource consumption rate is 6.65% and the highest image processing accuracy is 98.23%. Also, the rainy, cloudy and

sunny environments have less impact on the system performance. In summary, the new system proposed in the study has the best overall performance, and has more stable and superior recognition capability compared with the same type of radar image processing system. The wide applicability and robustness of the research system are verified.

4. Conclusion

With the continuous advancement of technology, the technology of directing and filming basketball games is also constantly developing. To meet the modern audience's demand for high-definition and real-time competition images, a new radar image processing system based on space cloud computing architecture is established by studying the powerful computing capabilities of the SAR overall framework based on space cloud computing and the high-resolution advantages of the multi star index based variable scale imaging algorithm. Whether in the GMTSAR dataset or the DORiSAR dataset, the research algorithm performed the best, with a maximum SSIM value of 0.99, which was very close to 1. The generated radar images were visually very close to the original images, and there was almost no obvious quality difference visible to the naked eye, indicating its significant advantage in maintaining image structure and quality. The simulation test results showed that the real-time data processing capability of space cloud computing and the ability to simplify complex processes through multi satellite connection state diagrams effectively enhance the responsiveness of radar image processing systems. The transmission time of the research system was only 2.2 seconds. As the number of runs increased, the increase in transmission time was very small, which did not affect the overall performance of the system. The complexity of operation was low, the calculation was simple, and it could efficiently process basketball game guidance and camera data. In summary, the excellent performance of the research system in terms of stability and real-time performance could make it a breakthrough technology in the field of basketball game guidance and filming. The research system's high-resolution imaging capability, combined with the efficient data processing of space cloud computing, provides a new technological platform for sports event broadcasting. However, the study did not include more complex basketball game director camera data for testing. Subsequent research can further optimize the algorithm by reducing the system's dependence on computing resources and incorporating more complex basketball game guidance camera data to enhance the comprehensiveness of the study. There are also a number of challenges in the actual deployment and maintenance of the research system. First, the deployment cost is high, mainly due to the need for high-performance GPUs, storage devices, and cloud computing infrastructure, which require large initial investments in equipment and technology. Maintenance challenges mainly include hardware management (e.g., GPU cooling, storage scaling), data security and system optimisation, especially the need to optimise algorithms to reduce dependence on computing resources

when faced with complex data. In terms of commercial potential, the system is capable of delivering high-definition, real-time game footage, which meets the high technological requirements of sports events and therefore has wide market demand. As the technology matures and cost and maintenance issues are resolved, the system is expected to become one of the core technologies for event broadcasting.

Author's declarations

Conflict of interest

The author has no conflict of interest to report.

Data availability

The information on the data sources are included in the manuscript in Section 3.1.

References

[1] B. Alouffi, M. Hasnain, A. Alharbi, W. Alosaimi, H. Alyami, et al. A systematic literature review on cloud computing security: Threats and mitigation strategies. *IEEE Access* 9(5):57792–57807, 2021. doi:10.1109/ACCESS.2021.3073203.

[2] N. M. Alsharari. Cloud computing and ERP assimilation in the public sector: institutional perspectives. *Transforming Government: People, Process and Policy* 16(1):97–109, 2022. doi:10.1108/TG-04-2021-0069.

[3] R. M. Asiyabi, A. Ghorbanian, S. N. Tameh, M. Amani, S. Jin, et al. Synthetic aperture radar (SAR) for ocean: A review. *IEEE Journal of Selected Topics in Applied Earth Observations and Remote Sensing* 16(4):9106–9138, 2023. doi:10.1109/JSTARS.2023.3310363.

[4] A. R. A. Besari, A. A. Saputra, W. H. Chin, Kurnianingsih, and N. Kubota. Finger joint angle estimation with visual attention for rehabilitation support: A case study of the chopsticks manipulation test. *IEEE Access* 10(94):91316–91331, 2022. doi:10.1109/ACCESS.2022.3201894.

[5] K. Cao, S. Hu, Y. Shi, A. W. Colombo, S. Karnouskos, et al. A survey on edge and edge-cloud computing assisted cyber-physical systems. *IEEE Transactions on Industrial Informatics* 17(11):7806–7819, 2021. doi:10.1109/TII.2021.3073066.

[6] J. Chen, M. Xing, H. Yu, B. Liang, J. Peng, et al. Motion compensation/autofocus in airborne Synthetic Aperture Radar: A review. *IEEE Geoscience and Remote Sensing Magazine* 10(1):185–206, 2022. doi:10.1109/MGRS.2021.3113982.

[7] M. Dai, Z. Su, R. Li, and S. Yu. A software-defined-networking-enabled approach for edge-cloud computing in the Internet of Things. *IEEE Network* 35(5):66–73, 2021. doi:10.1109/MNET.101.2100052.

[8] Y. Deng. Optimising enterprise financial sharing process using cloud computing and big data approaches. *International Journal of Grid and Utility Computing* 13(4):272–281, 2022. doi:10.1504/ijguc.2022.10049066.

[9] Y. Ding, Y. Shao, and J. Zhang. A cloud computing platform technology based on space-based intelligent information network. *Journal of Physics: Conference Series* 2203(1):12–22, 2022. doi:10.1088/1742-6596/2203/1/012042.

[10] N. Fu, S. Yun, B. Han, and L. Qiao. Sub-Nyquist measurement of LFM pulse stream based on signal separation and parameter matching. *IEEE Transactions on Instrumentation and Measurement* 72(6506015):1–15, 2023. doi:10.1109/TIM.2023.3328704.

[11] X. Gao, S. Roy, and G. Xing. MIMO-SAR: A hierarchical high-resolution imaging algorithm for mmWave FMCW radar in autonomous driving. *IEEE Transactions on Vehicular Technology* 70(8):7322–7334, 2021. doi:10.1109/TVT.2021.3092355.

[12] M. Gottinger. Coherent automotive radar networks: The next generation of radar-based imaging and mapping. *IEEE Journal of Microwaves* 1(1):149–163, 2021. doi:10.1109/JMW.2020.3034475.

[13] J. P. Hati, A. Mukhopadhyay, and N. R. Chaube. Estimation of above ground biomass with synthetic aperture radar (SAR) data in Lothian Island, Sundarbans, India. *Journal of the Indian Society of Remote Sensing* 52(4):757–769, 2024. doi:10.1007/s12524-023-01788-9.

[14] Y. Huang, Z. Chen, C. Wen, J. Li, X. G. Xia, et al. An efficient radio frequency interference mitigation algorithm in real Synthetic Aperture Radar data. *IEEE Transactions on Geoscience and Remote Sensing* 60(4):5224912, 2022. doi:10.1109/TGRS.2022.3155068.

[15] M. Jing and G. Zhang. Location of synthetic aperture radar imagery via range history. *IEEE Transactions on Geoscience and Remote Sensing* 60:5232112, 2022. doi:10.1109/TGRS.2022.3192984.

[16] N. Kikon, D. Kumar, and S. A. Ahmed. Spaceborne synthetic aperture radar (SAR) earth observations for surface deformation analysis and mapping. *Arabian Journal of Geosciences* 15:1131, 2022. doi:10.1007/s12517-022-10370-5.

[17] A. Kittel, P. Larkin, and N. Elsworthy. Transfer of 360 virtual reality and match broadcast video-based tests to on-field decision-making. *Science and Medicine in Football* 5(1):79–86, 2021. doi:10.1080/24733938.2020.1802506.

[18] D. Kumar. Urban objects detection from C-band synthetic aperture radar (SAR) satellite images through simulating filter properties. *Scientific Reports* 11(1):21–30, 2021. doi:10.1038/s41598-021-85121-9.

[19] B. Li and X. Xu. Application of Artificial Intelligence in basketball sport. *Journal of Education, Health and Sport* 11(7):54–67, 2021. doi:10.12775/JEHS.2021.11.07.005.

[20] K. Li. Ding Xilin's Chinese translation of The Man of Destiny: Reading Shaw through IBM Artificial Intelligence and Cloud Computing Platform. *Shaw* 41(1):151–166, 2021. doi:10.5325/SHAW.41.1.0151.

[21] N. Li, Z. Lv, and Z. Guo. Pulse RFI mitigation in Synthetic Aperture Radar data via a three-step approach: Location, Notch, and Recovery. *IEEE Transactions on Geoscience and Remote Sensing* 60:5225617, 2022. doi:10.1109/TGRS.2022.3161368.

[22] A. Liu, N. Wang, D. Dettmering, Z. Li, M. Schmidt, et al. Using DORIS data for validating real-time GNSS ionosphere maps. *Advances in Space Research* 71(1):115–128, 2023. doi:10.1016/j.asr.2023.01.050.

[23] A. Madankan. The response time analysis of queuing model in cloud computing environment. *Computer Science Journal of Moldova* 30(4):64–76, 2022. doi:10.56415/csjm.v30.04.

[24] D. Mao. Forward-looking geometric configuration optimization design for spaceborne-airborne multistatic Synthetic Aperture Radar. *IEEE Journal of Selected Topics in Applied Earth Observations and Remote Sensing* 14(4):8033–8047, 2021. doi:10.1109/JSTARS.2021.3103802.

[25] A. Nuriddinov. Use of digital sports technologies in sports television. *American Journal Of Social Sciences And Humanity Research* 3(11):208–219, 2023. doi:10.37547/ajsshr/Volume03Issue11-22. https://inlibrary.uz/index.php/ajsshr/article/view/38358.

[26] E. N. Oh, M. R. Baharon, S. M. W. M. S. M. M. Yassin, A. Idris, and A. MacDermott. Preserving data privacy in mobile cloud computing using enhanced homomorphic encryption scheme. *Journal of Physics: Conference Series* 2319:012024, 2022. doi:10.1088/1742-6596/2319/1/012024.

[27] P. Pięta, H. Jegierski, P. Babiuch, M. Jegierski, M. Płaza, et al. Automated classification of virtual reality user motions using a motion atlas and machine learning approach. *IEEE Access* 12:94584–94609, 2024. doi:10.1109/ACCESS.2024.3424930.

[28] D. Sandwell, R. Mellors, X. Tong, M. Wei, and P. Wessel. Open radar interferometry software for mapping surface deformation. *Eos, Transactions American Geophysical Union* 92(28):234–234, 2011. doi:10.1029/2011EO280002.

[29] D. Sandwell, X. E. Xu, R. Mellors, X. Tong, and M. M. Wei. An InSAR processing system based on GMT. GMTSAR, 2010. https://topex.ucsd.edu/gmtsar/.

[30] T. A. Sleem, A. M. Hegazi, and A. M. Zaki. Integration of historical synthetic aperture radar (SAR) and geotechnical data for monitoring ground instability: a case study of Ismailia District, Egypt. *Arabian Journal of Geosciences* 15(1):100, 2022. doi:10.1007/s12517-021-09142-4.

[31] E. F. Smirnov, N. S. Ivanov, M. Zavgorodnii, I. Y. Khramov, and V. V. Chernyshova. Recognition of the basketball players position using live cameras. In: *2021 IEEE Conference of Russian Young Researchers in Electrical and Electronic Engineering (ElConRus)*, pp. 695–698, 2021. doi:10.1109/ElConRus51938.2021.9396214.

[32] The MathWorks, Inc. MATLAB. Natick, MA, USA. https://www.mathworks.com.

[33] N. Tomii. Infrastructure monitoring by satellite based synthetic aperture radar (SAR) in JAXA. *Artificial Intelligence and Data Science* 4(1):3–8, 2023. doi:10.11532/jsceiii.4.L1_3.

[34] Z. Wei, N. Fu, S. Jiang, X. Li, and L. Qiao. Parameter measurement of LFM signal with FRI sampling and nuclear norm denoising. *IEEE Transactions on Instrumentation and Measurement* 71:2002417, 2022. doi:10.1109/TIM.2022.3158986.

[35] G. Xu, B. Zhang, H. Yu, J. Chen, M. Xing, et al. Sparse Synthetic Aperture Radar imaging from compressed sensing and machine learning: Theories, applications, and trends. *IEEE Geoscience and Remote Sensing Magazine* 10(4):32–69, 2022. doi:10.1109/MGRS.2022.3218801.

[36] C. Yan, B. Gong, Y. Wei, and Y. Gao. Deep multi-view enhancement hashing for image retrieval. *IEEE Transactions on Pattern Analysis and Machine Intelligence* 43(4):1445–1451, 2020. doi:10.1109/TPAMI.2020.2975798.

[37] C. Yan, Y. Hao, L. Li, J. Yin, A. Liu, et al. Task-adaptive attention for image captioning. *IEEE Transactions on Circuits and Systems for Video Technology* 32(1):43–51, 2021. doi:10.1109/TCSVT.2021.3067449.

[38] C. Yan, Z. Li, Y. Zhang, Y. Liu, X. Ji, et al. Depth image denoising using nuclear norm and learning graph model. *ACM Transactions on Multimedia Computing Communications and Applications* 16(4):1–17, 2020. doi:https://doi.org/10.1145/3404374.

[39] C. Yan, L. Meng, L. Li, J. Zhang, J. Yin, et al. Age-invariant face recognition by multi-feature fusion and decomposition with self-attention. *ACM Transactions on Multimedia Computing Communications and Applications* 18(1):1–18, 2021. doi:https://doi.org/10.1145/3472810.

[40] C. Yan, Y. Sun, H. Zhong, C. Zhu, Z. Zhu, et al. Review of omnimedia content quality evaluation. *Journal of Signal Processing* 38(6):1111–1143, 2022. doi:10.16798/j.issn.1003-0530.2022.06.001. https://signal.ejournal.org.cn/article/doi/10.16798/j.issn.1003-0530.2022.06.001.

[41] C. Yan, T. Teng, Y. Liu, Y. Zhang, H. Wang, et al. Precise no-reference image quality evaluation based on distortion identification. *ACM Transactions on Multimedia Computing Communications and Applications* 17(3s):110, 2021. doi:10.1145/3468872.

[42] M. Younis, F. Q. de Almeida, M. Villano, S. Huber, G. Krieger, et al. Digital beamforming for spaceborne Reflector-Based Synthetic Aperture Radar, Part 1: Basic imaging modes. *IEEE Geoscience and Remote Sensing Magazine* 9(3):8–25, 2021. doi:10.1109/MGRS.2021.3060543.

[43] Y. Yuan, S. Chen, Y. Zhang, S. Wang, and S. Zhang. Nonlinear chirp scaling imaging method for three-dimensional foresight linear array maneuvering SAR. *IEEE Transactions on Geoscience and Remote Sensing* 60:5233913, 2022. doi:10.1109/TGRS.2022.3200973.

[44] Z. Zhang, L. Li, G. Cong, H. Yin, Y. Gao, et al. From speaker to dubber: Movie dubbing with prosody and duration consistency learning. In: *Proceedings of the 32nd ACM International Conference on Multimedia*, MM '24, p. 7523–7532. Association for Computing Machinery, New York, NY, USA, 2024. doi:10.1145/3664647.3680777.